J. Min. Metall. Sect. B-Metall., 56 (1) (2020) 35 - 42

Journal of Mining and Metallurgy, Section B: Metallurgy

EVALUATION OF CARBIDE CAPACITY IN CaO-BASED TERNARY SYSTEMS AT 1773K FOR REFINING PROCESS

Z.-G. Yu [a], H.-Y. Leng [a], L.-J. Wang [b], K.-C. Chou [a,*]

[a] State Key Laboratory of Advanced Special Steel & Shanghai Key Laboratory of Advanced Ferrometallurgy & School of Materials Science and Engineering, Shanghai University, Shanghai, China
[b] State Key Laboratory of Advanced Metallurgy & Collaborative Innovation Center of Steel Technology, University of Science and Technology Beijing, Beijing, China

(Received 10 January 2019; accepted 17 October 2019)

Abstract

Refining slags is widely used in the production of high-value-added alloys and special steels. The removal of impurities depends on the mass transfer between the slag-metal interface, and the carbide capacity of the refining slags is crucial to control the carbon content in the final products. A phenomenological model is introduced in this article for the calculation of carbide capacity of different CaO-based ternary refining slags. The contour lines of carbide capacity in CaO-Al_2O_3-CaF_2, CaO-SiO_2-CaF_2 CaO-SiO_2-MnO systems are calculated based on limited experimental data by the present model. The experimental data within the calculation boundary are compared with the predicted values and satisfactory agreements are observed with the mean deviation being 1.4%, 2.3%, and 1.6%, for these three systems respectively. The present model is powerful and flexible in the calculation of carbide capacity of CaO-based ternary refining slags and can be applied to other systems.

Keywords: *Carbide capacity; Prediction; Model; CaO-based; Refining slags*

1. Introduction

The key to the production of special steels or superalloys lies in the removal of impurities in the molten metal [1, 2]. The existence of carbon in steels causes brittle fractures of steel in extreme conditions, which need to be removed through the refining process [3]. Carbon removal by slag refining isn't the priority in steelmaking, but can be more important in other alloys, such as ferrochrome [4, 5] and ferromanganese [6] alloys. The removal of carbon depends on the mass transfer between the slag-metal interface when the hot metal drops cross the slag layer and fall into the molten pool [7, 8]. As a result, the carbide capacity of the refining slags is crucial to the control of the carbon content in the final products. However, most of the refining slag systems are with high melting points and can corrode the crucible at high temperatures, so it is impossible to obtain all these carbide capacity data for practical use just through experimental methods.

On the contrary, the model prediction is an alternative which may address this issue in a more effective way. The geometrical model [9-11] is a powerful tool to predict the properties of slags and has been widely used in the calculation of sulfide capacities [12-14], phosphate capacities [15], and other physicochemical properties of slags [15-27]. Traditional geometrical models [9, 11, 28-32] can predict the properties of ternary systems only when the binary data are abundant. However, most of the slag systems are with miscibility gaps at their application temperature, where the limited solubility area doesn't even intersect with the binary boundaries. So, on this condition, these systems are not suitable to be calculated by traditional geometrical models for the lack of corresponding binary data.

Recently, Chou [33-35] has extended the geometrical model to the systems with limited solubility area by proposing a new method. The new method can predict the physicochemical properties of ternary systems just based on limited experimental boundary data, which will enlarge the application range of geometrical models in practical systems. In this article, our new model will be first applied into the calculation of carbide capacity of ternary slags for refining process. The predicted results show good agreements with the experimental data in CaO-Al_2O_3-CaF_2, CaO-SiO_2-CaF_2 CaO-SiO_2-MnO slag systems. The contour lines of carbide capacity for different systems are also calculated by the present model.

*Corresponding author: kcc126@126.com

https://doi.org/10.2298/JMMB190110054Y

2. Model description

According to the new model [33-35], there are three conditions: limited binary boundary data, limited ternary boundary data, and even only three experimental data, which can be used for calculation of the systems with limited solubility. A short description of the second condition that calculation based on limited ternary boundary data will be given here.

As illustrated in Fig. 1, the gray part is the limited solubility area, which has no interaction with the binary boundary. The dash line along the limited solubility area is the calculation boundary, which is not a real boundary and can be arbitrarily selected according to the distribution of the experimental points. The physicochemical properties can be calculated within this boundary when choosing three points ("A" "B" "C") on this calculation boundary for the calculation, and the selection rule of the three calculation points (A" "B" "C") can just follow Chou's method [28]. Then, the properties of point "O" are calculated by a combination of the three calculation points ("A" "B" "C") according to the equations below.

$$\Delta P_o = W_A \Delta P_A + W_B \Delta P_B + W_C \Delta P_C \quad (1)$$

where ΔP_i is the physicochemical property of point "i", and W_A, W_B, W_C is the corresponding weight probability of different calculation points (A" "B" "C"). In the present model, the weight probability of each calculation point can be expressed as the following equations.

$$W_A = \frac{(x_1^O - x_1^B)(x_2^O - x_2^C)}{\sqrt{(x_1^O - x_1^B)^2 + (x_3^O - x_3^A)^2 + (x_1^O - x_1^B)(x_3^O - x_3^A)}\sqrt{(x_2^O - x_2^C)^2 + (x_3^O - x_3^A)^2 + (x_2^O - x_2^C)(x_3^O - x_3^A)}} \quad (2)$$

$$W_B = \frac{(x_3^O - x_3^A)(x_2^O - x_2^C)}{\sqrt{(x_1^O - x_1^B)^2 + (x_3^O - x_3^A)^2 + (x_1^O - x_1^B)(x_3^O - x_3^A)}\sqrt{(x_1^O - x_1^B)^2 + (x_2^O - x_2^C)^2 + (x_1^O - x_1^B)(x_2^O - x_2^C)}} \quad (3)$$

$$W_C = \frac{(x_3^O - x_3^A)(x_1^O - x_1^B)}{\sqrt{(x_2^O - x_2^C)^2 + (x_3^O - x_3^A)^2 + (x_2^O - x_2^C)(x_3^O - x_3^A)}\sqrt{(x_1^O - x_1^B)^2 + (x_2^O - x_2^C)^2 + (x_1^O - x_1^B)(x_2^O - x_2^C)}} \quad (4)$$

where x_j^i is the composition of "j, at point "i", and the weight probabilities of the calculation points are expressed as the component coordinates of each point. In Fig.1, the distance between point "O" and points "A" "B" "C" are OA= $x_3^O - x_3^A$, OB= $x_1^O - x_1^B$, and OC= $x_2^O - x_2^C$. It is easy to find that the weight probabilities of the calculation points just depend on their distances from point "O". The nearer the calculation point ("A" or "B" or "C") is to the calculated point "O", the larger the weight probability is. Combined with the equation (1), as a result, the property between the calculation point ("A" or "B" or "C") and point "O" will be more similar, which is reasonable and consistent with the reality. The detailed theoretical derivation process can be referred to our previous article [35].

3. Carbide capacity prediction of various systems

The measurement of carbide capacity is difficult due to the high melting points of the refining slags and the experimental data varies when it is measured by different researchers, which brings difficulties for model prediction. Park et al. [36-38] measured the carbide capacity of different systems and determined the content of carbon in the slags by a LECO (CS-300) analyzer. All the carbide capacity data measured by Park et al. were chosen for the calculation in the following examples. First, the outmost layer experimental data were selected as the calculation boundary (Bi, i≥3) and the inner data as the calculated points (Ci) for the comparison. All the calculation data of the present model are along the virtual ternary boundary, and all the calculated contour lines of carbide capacity are with the same range of notation to have an intuitive comparison of different systems.

The relative deviation (R.D.) and mean deviation (Δ) were used to compare the inner experimental data (Ci) with the calculated values, as expressed in the equation below:

$$R.D. = \frac{C_{\text{Carbide}}^{Cal.} - C_{\text{Carbide}}^{Exp.}}{C_{\text{Carbide}}^{Exp.}} \times 100\% \quad (5)$$

$$\Delta = \frac{1}{N}\sum_{n=1}^{N} |R.D| \quad (6)$$

where $C_{\text{Carbide}}^{Cal.}$ and $C_{\text{Carbide}}^{Exp.}$ are the calculated (Cal.) carbide capacity and experimental (Exp.) values, respectively. N is the number of comparison data.

3.1 $CaO-Al_2O_3-CaF_2$ ternary system

$CaO-Al_2O_3-CaF_2$ slag is the most basic ternary system for ESR process, and has been widely used in the production of special steels. Park et al. [36] measured the carbide capacity of this system in a wide composition range within the limited solubility area at 1773K. Seventeen experimental data were chosen as the calculation boundary points, as set out in Table 1. All these calculation points were located at the outmost layer of the composition triangle among all the experimental data and constituted a virtual calculation boundary (Fig. 2). Combined with the equations (1-4), the carbide capacity could be predicted within this calculation boundary. As shown in Fig. 2, the contour lines of carbide capacity in $CaO-Al_2O_3-CaF_2$ system at 1773K were calculated by the present model.

The experimental data [36] within the calculation boundary (C1-C7) were selected to compare with the calculated values. As illustrated in Fig. 2, the comparison points (C1-C7) are marked in red and uniformly distributed inside the calculation boundary. The detailed comparison results between the experimental carbide capacity and the calculated values of each point are listed in Table 2. The relative deviation (R.D.) ranges from -0.4% to -2.5%, with the mean deviation (Δ) being 1.4% for seven groups of data.

Besides, the predicted results along three component lines of $CaO-Al_2O_3-CaF_2$ ternary system were chosen to show the influence of different additions on the carbide capacity of this system. As depicted in Fig. 3, when the content of CaF_2 or CaO is 0.3 (30 mol.%), the addition of Al_2O_3 decreases the carbide capacity of $CaO-Al_2O_3-CaF_2$ ternary system, especially when the content of CaF_2 is constant (red points in Fig. 3). However, the addition of CaF_2 shows a slight effect on the carbide capacity of $CaO-Al_2O_3$-

Table 1. *Calculation boundary data of carbide capacity (B1-B17) in $CaO-Al_2O_3-CaF_2$ slag within the limited solubility region at 1773K by Park [36] work [10]*

Points	Composition (mole fraction)			log $C_{carbide}$
	Al_2O_3	CaF_2	CaO	
B1	0	0.695	0.305	-8.27
B2	0.425	0.283	0.292	-9.03
B3	0.426	0.268	0.306	-9.08
B4	0.411	0.193	0.396	-9.02
B5	0.408	0.179	0.413	-9.04
B6	0.407	0.148	0.445	-8.83
B7	0.268	0.011	0.721	-8.89
B8	0.264	0.008	0.728	-8.78
B9	0.223	0.086	0.691	-8.56
B10	0.227	0.096	0.677	-8.67
B11	0.201	0.141	0.658	-8.48
B12	0.217	0.14	0.643	-8.49
B13	0.153	0.24	0.607	-8.28
B14	0.131	0.357	0.512	-8.16
B15	0.131	0.365	0.504	-8.21
B16	0.046	0.557	0.397	-8.24
B17	0	0.679	0.321	-8.18

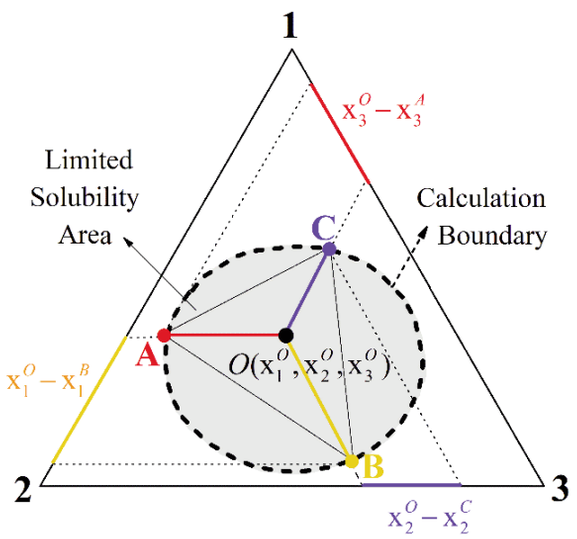

Figure 1. *The schematic diagram for calculating liquid properties based on boundary data of the systems with limited solubility area*

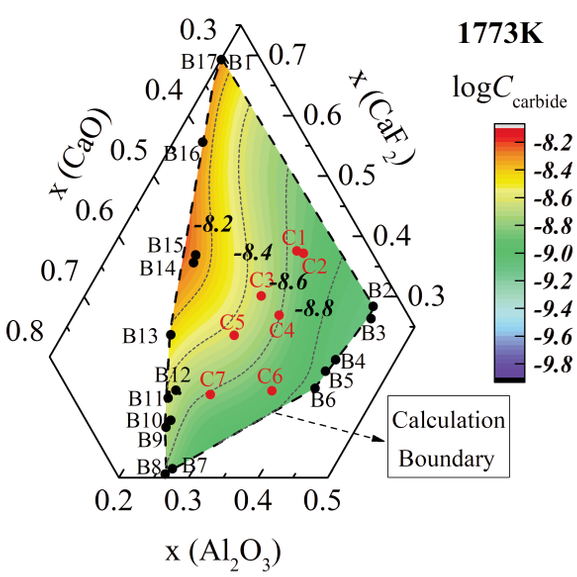

Figure 2. *The calculated contour lines of carbide capacity in $CaO-Al_2O_3-CaF_2$ slag by the present model at 1773K*

Table 2. *The relative deviation (R.D.) and mean deviation (Δ) between the inner experimental carbide capacity data (C1-C7) [36] and the calculated values by the present model*

Points	Composition (mole fraction)			log $C_{carbide}$		R.D.
	Al_2O_3	CaF_2	CaO	Exp.	Cal.	
C1	0.268	0.375	0.357	-8.84	-8.88	-0.40%
C2	0.27	0.376	0.354	-8.85	-8.89	-0.40%
C3	0.254	0.303	0.443	-8.56	-8.69	-1.60%
C4	0.296	0.27	0.434	-8.67	-8.83	-1.80%
C5	0.248	0.235	0.517	-8.55	-8.64	-1.00%
C6	0.348	0.144	0.508	-8.88	-9.05	-1.90%
C7	0.263	0.138	0.599	-8.61	-8.83	-2.50%
				Δ		**1.40%**

CaF_2 ternary system when the content of Al_2O_3 is constant (black points in Fig. 3). It can be concluded that, if one wants to increase the carbide capacity of CaO-Al_2O_3-CaF_2 slag system for ESR, the content of Al_2O_3 needs to be reduced.

3.2 CaO-SiO_2-CaF_2 ternary system

Silicate slags are extensively used to control the removal process of boron from molten silicon, and CaO-SiO_2-CaF_2 is a basic silicate slag system in the refining process of metallurgical-grade silicon [39-41]. Park et al. [37] also measured the carbide capacity of this system within the limited solubility area at 1773K. Because the 20 experimental points were not evenly distributed, just 6 of them located at the outmost layer of the composition triangle were chosen as the calculation boundary points (B1-B6). The calculation boundary points are listed in Table 1 and constitute the calculation boundary in Fig. 2. Combined with the above equations (1-4), the contour lines of carbide capacity in CaO-SiO_2-CaF_2 system at 1773K were predicted, as shown in Fig. 2. The contour lines are much denser than that of CaO-Al_2O_3-CaF_2 system in Fig. 2, which means the carbide capacity changes more dramatically in CaO-SiO_2-CaF_2 system.

The comparison results between the experimental carbide capacity [37] and the calculated values are shown in Table 3. As illustrated in Fig.4, all the comparison points (C1-C14) are within the calculation boundary, marked in red. Although the calculation boundary points are very limited, the predicted results still agree well with the experimental ones, with the mean deviation (Δ) being 2.3% for 14 groups of data. This result proves the reliability of the present model, even under the conditions with very limited experimental data. It reveals the potential application value of the present model because the

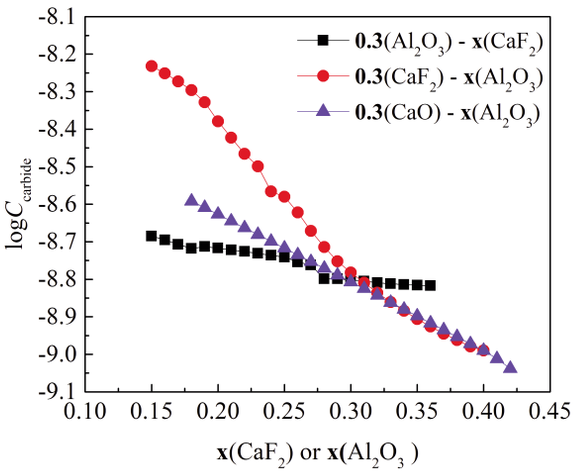

Figure 3. *The predicted carbide capacity along different component lines of CaO-Al_2O_3-CaF_2 slag at 1773K*

experimental data of most slag systems are scarce and scattered.

In addition, the predicted results along three component lines of CaO-Al_2O_3-CaF_2 ternary system are also illustrated in Fig.5 to show the influence of different additions on the carbide capacity of this system. It can be seen from Fig. 5 that the addition of SiO_2 decreases the carbide capacity dramatically when the content of CaF_2 or CaO is constant (0.3 CaF_2 or 0.5CaO), while the addition of CaF_2 increases the carbide capacity of CaO-SiO_2-CaF_2 ternary system slightly, when the content of SiO_2 is constant (0.3SiO_2, black points in Fig. 5). Combined with the results of CaO-Al_2O_3-CaF_2 system in Fig.3, it is easy to find that SiO_2 and Al_2O_3 show the similar influence on the carbide capacity of CaO-CaF_2-based ternary system, which can be explained that SiO_2 is a kind of acid oxides and Al_2O_3, which is a kind of amphoteric oxides, exhibits the characteristics of acidic oxides with high content CaO. As illustrated in Fig. 5, the reduction of SiO_2 results in the increase of carbide capacity of 0.3CaF_2-x(SiO_2) and 0.5CaO-x(SiO_2) systems.

3.3 CaO-SiO_2-MnO ternary system

The manganese-rich slag, generated from the high carbon ferromanganese production process, has the advantage of low phosphorus content, and CaO-SiO_2-MnO slag is a good alternative to producing silicomanganese alloys. The carbide capacity of this system, which was measured by Park et al. [38] at 1773K, is critical to the carbide content of the final products. We selected 11 of the experimental points as the calculation boundary (B1-B11 in Table 5), and 8 of them as the comparison points (C1-C8 in Table 6). All the experimental points are shown in Fig. 6, where

Table 3. *Calculation boundary data of carbide capacity (B1-B6) in SiO_2-CaF_2-CaO slag within the limited solubility region at 1773K by Park [37]*

Points	Composition (mole fraction)			log $C_{carbide}$
	SiO_2	CaF_2	CaO	
B1	0.551	0.361	0.087	-9.49
B2	0.392	0.088	0.521	-9.03
B3	0.218	0.13	0.651	-8.52
B4	0.178	0.136	0.686	-8.51
B5	0.155	0.27	0.575	-8.32
B6	0.174	0.376	0.45	-8.17

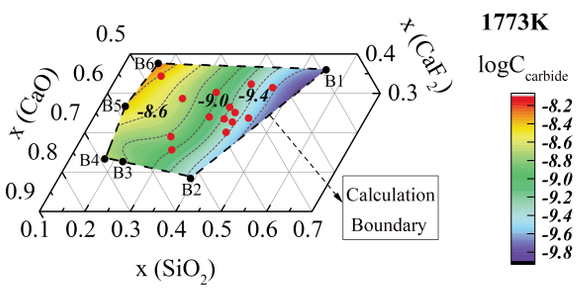

Figure 4. *The calculated contour lines of carbide capacity in CaO-SiO_2-CaF_2 slag by the present model at 1773K*

the 11 points of the outmost layer constitute a virtual boundary, and the 8 comparison points are within this boundary.

We predicted the contour lines of carbide capacity in CaO-SiO_2-MnO system at 1773K, according to equations (1-4). As shown in Fig. 6, the contour lines are not as regular as those of CaO-Al_2O_3-CaF_2 or CaO-SiO_2-CaF_2 system above, which means that the carbide capacity changes may not be linear with the addition of the oxide. Also, the predicted results along three component lines of CaO-SiO_2-MnO ternary system just prove this inference. The influences of different additions on the carbide capacity of this system are depicted in Fig.7, where the existence of MnO results in irregular changes of the carbide capacity (black and blue points in Fig.7). When the content of MnO is restricted to 0.1(10mol.%), the addition of SiO_2 decreases the carbide capacity regularly (red points in Fig. 7). The irregular effect of MnO on the carbide capacity of CaO-SiO_2-MnO can be attributed to the abnormal-valence of Mn at high temperature. The reduction of the content of SiO_2 is easier to control if increasing the carbide capacity of CaO-SiO_2-MnO slag system is wanted.

The detailed comparison of the predicted results with the experimental values of the inner comparison points [38] are listed in Table 6. The relative deviation (R.D.) varies from -4.8% to 0.5%, with the mean

Table 4. *The relative deviation (R.D.) and mean deviation (Δ) between the inner experimental carbide capacity data (C1-C14) [37] and the calculated values by the present model*

Points	Composition (mole fraction)			log $C_{carbide}$		R.D.
	SiO_2	CaF_2	CaO	Exp.	Cal.	
C1	0.405	0.318	0.277	-9.16	-8.68	-5.30%
C2	0.194	0.345	0.461	-8.24	-8.82	-3.90%
C3	0.294	0.187	0.519	-8.49	-8.62	1.80%
C4	0.273	0.287	0.44	-8.77	-9.2	-2.90%
C5	0.393	0.262	0.345	-8.94	-9.34	-2.00%
C6	0.337	0.306	0.357	-9.35	-8.89	4.90%
C7	0.351	0.241	0.408	-9.28	-8.94	3.70%
C8	0.314	0.155	0.531	-8.93	-8.96	-0.30%
C9	0.409	0.204	0.387	-9.4	-9.3	1.10%
C10	0.408	0.228	0.364	-9.39	-9.25	1.50%
C11	0.396	0.232	0.372	-9.34	-9.18	1.70%
C12		0.255	0.344	-9.41	-9.22	2.00%
C13	0.44	0.234	0.326	-9.48	-9.47	0.20%
C14	0.457	0.311	0.232	-9.59	-9.63	-0.40%
				Δ		**2.30%**

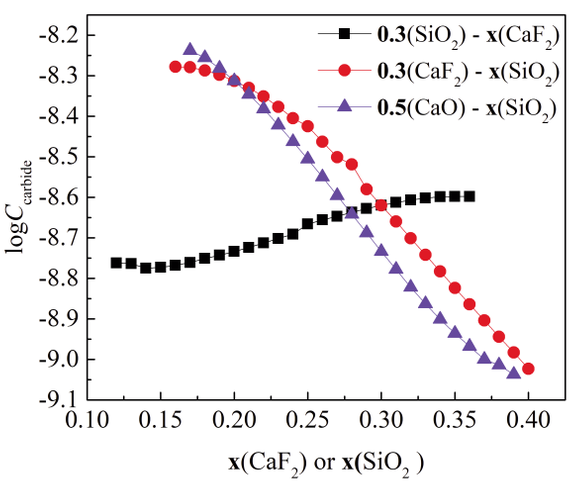

Figure 5. *The predicted carbide capacity along different component lines of SiO_2-CaF_2-CaO slag at 1773K*

deviation (Δ) being 1.6% for 8 groups of data, where the calculated results agree well with the experimental carbide capacity.

4. Discussion

In the three examples above, the distribution of the experimental points varies, but all the predicted results by the present model agree well with the

Table 5. *Calculation boundary data of carbide capacity (B1-B11) in SiO_2-MnO-CaO slag within the limited solubility region at 1773K by Park [38]*

Points	Composition (mole fraction)			log $C_{carbide}$
	SiO_2	MnO	CaO	
B1	0.598	0.229	0.173	-9.58
B2	0.59	0.189	0.221	-9.72
B3	0.606	0.153	0.242	-9.51
B4	0.626	0	0.374	-9.43
B5	0.564	0	0.436	-9.48
B6	0.465	0	0.535	-9.31
B7	0.396	0	0.604	-8.92
B8	0.404	0.036	0.559	-8.71
B9	0.423	0.142	0.436	-9.3
B10	0.446	0.217	0.336	-9.29
B11	0.535	0.227	0.238	-9.48

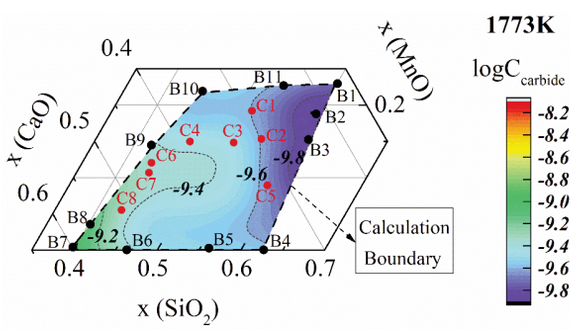

Figure 6. *The calculated contour lines of carbide capacity in CaO-SiO_2-MnO slag by the present model at 1773K.*

experimental values, which means the present model is powerful in the prediction of the carbide capacity of slags and can be applied to more systems. Theoretically, the denser the calculation boundary points are, the higher the prediction accuracy is, which was proved by the results in the examples above. Besides, the selection of the calculation boundary is flexible and has no need to be restricted to the binary boundaries, which enlarge the application range of geometrical models extensively.

We calculated the contour lines of carbide capacity within the calculation boundary and the carbide capacity along different component lines to show the influences of diverse components. It can be concluded that the reduction of SiO_2 or Al_2O_3 will be of help for the increase of carbide capacity of CaO-based systems, while the CaF_2 shows slight influence. Besides, the addition of MnO shows irregular influence due to the abnormal-valence of Mn at high temperature.

Table 6. *The relative deviation (R.D.) and mean deviation (Δ) between the inner experimental carbide capacity data (C1-C8) [38] and the calculated values by the present model*

Points	Composition (mole fraction)			log $C_{carbide}$		R.D.
	SiO_2	MnO	CaO	Exp.	Cal.	
C1	0.515	0.194	0.291	-9.38	-9.6	-2.40%
C2	0.547	0.156	0.297	-9.53	-9.58	-0.60%
C3	0.517	0.15	0.334	-9.24	-9.45	-2.30%
C4	0.466	0.148	0.386	-9.08	-9.52	-4.80%
C5	0.587	0.089	0.325	-9.59	-9.61	-0.20%
C6	0.435	0.118	0.447	-9.42	-9.37	0.50%
C7	0.436	0.109	0.455	-9.38	-9.32	0.60%
C8	0.43	0.057	0.514	-9.5	-9.34	1.70%
				Δ		**1.60%**

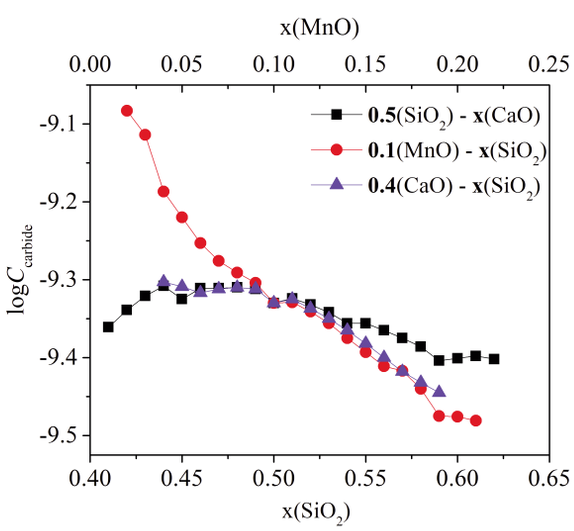

Figure 7. *The predicted carbide capacity along different component lines of CaO-SiO_2-MnO slag at 1773K.*

5. Conclusion

In this article, an extended geometrical model is applied to the calculation of the carbide capacity, of CaO-Al_2O_3-CaF_2, CaO-SiO_2-CaF_2, and CaO-SiO_2-MnO systems for the refining process. Satisfactory agreements between the experimental data and the calculated values are observed. In addition, the contour lines of carbide capacity in all three systems are predicted based on limited experimental data by the present model. The selection of the calculation boundary is flexible and has no need to be restricted to the binary boundaries, which enlarges the application range of geometrical models extensively.

More applications in the calculation of carbide capacity will be extended to other systems, except for the CaO-based refining slags, in our coming papers.

Acknowledgements

This work was financially supported by the National Natural Science Foundation of China (Nos.51734002, 51474141).

References

[1] J. Burja, F. Tehovnik, M. Godec, J. Medved, B. Podgornik,R. Barbic, J. Min. Metall. Sect. B-Metall., 54(1)(2018)51-57.

[2] V. Weber, A. Jardy, B. Dussoubs, D. Ablitzer, S. Rybéron, V. Schmitt, S. Hans,H. Poisson, Metall. Mater. Trans. B, 40(3)(2009)271-280.

[3] H. Wang, M.M. Nzotta, L. Teng,S. Seetharaman, J. Min. Metall. Sect. B-Metall., 49(2)(2013)175-181.

[4] T. Hu, H. Liu, B. Liu, L. Dai, L. Zhang,S. Guo, 10th International Symposium on High-Temperature Metallurgical Processing, San Antonio, Texas, USA,2019,p.349-359.

[5] H. Weitz,A.M. Garbers Craig, Miner. Process. Extr. Metall. Rev., 37(3)(2016)168-178.

[6] H.S. Jang, J.W. Ryu,I. Sohn, Metall. Mater. Trans. B, 46(2)(2014)606-614.

[7] A. Kharicha, M. Wu, A. Ludwig, E. K. Sibaki, Metall. Mater. Trans. B, 47(2)(2016)1427-1434.

[8] A.W. Bydalek, J. Therm. Anal. Calorim., 65(2)(2001)591-597.

[9] K.C. Chou,Y.A. Chang, Ber. Bunsengesell. Phys. Chem., 93(6)(1989)735-741.

[10] K.C. Chou, ISIJ Int., 58(5)(2018)785-791.

[11] K.C. Chou, Calphad, 19(3)(1995)315-325.

[12] L.J. Wang, Q.Y. Liu, K.C. Chou, J. Min. Metall. Sect. B-Metall., 48(2)(2012)219-226.

[13] Y. Wang, L. Wang, K.C. Chou, High Temp. Mater. Process, 36(6)(2016)1-5.

[14] Z.G. Yu, H.Y. Leng, L.J. Wang, K.C. Chou, Ceram. Int., 45(6)(2019)7180-7187.

[15] Y. Sun, L. Wang, J. Xu, K. Chou, J. Min. Metall. Sect. B-Metall., 53(1)(2017)31-36.

[16] D. Živković,D. Manasijević, Calphad, 29(4)(2005)312-316.

[17] G.H. Zhang, L.J. Wang,K.C. Chou, Calphad, 34(4)(2010)504-509.

[18] Z.Y. Chen, J.H. Liu, Z.Y. Yu,K.C. Chou, Thermochim. Acta, 543(1)(2012)107-112.

[19] L. Wang, K.C. Chou,S. Seetharaman, Calphad, 32(1)(2008)49-55.

[20] D. Živković, D. Minić, D. Manasijević, N. Talijan, I. Katayama,A. Kostov, J. Mater. Sci. Mater. Electron., 22(8)(2011)1130-1135.

[21] L. Gomidzelovic, D. Zivkovic, L. Balanovic,D. Manasijevic, Rare Metals, 35(3)(2016)262-268.

[22] P. Fima, R. Novakovic, Philos. Mag., 98 (17) (2018) 1608-1624.

[23] H. Arslan, A. Dogan, J. Fac. Eng. Archit. Gaz., 34(2)(2019)597-608.

[24] D. Zivkovic, D. Minic, D. Manasijevic, A. Kostov, N. Talijan, L. Balanovic, A. Mitovski,Z. Zivkovic, J. Min. Metall. Sect. B-Metall., 46(1)(2010)105-111.

[25] D. Minic, Y. Du, M. Premovic, D. Manasijevic, N. Talijan, D. Milisavljevic, A. Markovic, A. Djordjevic, M. Tomovic, J. Min. Metall. Sect. B-Metall., 53(3)(2017)189-201.

[26] Y. Du, J. Wang, Y.F. Ouyang, L.J. Zhang, Z.H. Yuan, S.H. Liu,P. Nash, J. Min. Metall. Sect. B-Metall., 46(1)(2010)1-9.

[27] Z.G. Yu, Q. Luo, J.Y. Zhang, K.C. Chou, Philos. Mag., 99(19)(2019)2408-2423.

[28] K.C. Chou, Calphad, 11(3)(1987)293-300.

[29] Y.M. Muggianu, M. Gambino, J.P. Bros, J. Chim. Phys., 72(1)(1975)83-88.

[30] M. Hillert, Calphad, 4(1)(1980)1-12.

[31] F. Kohler, Monatsh. Chem., 91(4)(1960)738-740.

[32] G.W. Toop, Trans. AIME, 233(5)(1965)850-855.

[33] K.C. Chou, Asia Steel International Conference, Oct.5-8,Yokohama, Japan,2015,p.32-33.

[34] K.C. Chou, The 4th China-United States Symposium on Energy, Jun. 25-27, Shanghai, China,2017,p.5.

[35] K.C. Chou,Z.G. Yu, Ceram. Int., 44 (17) (2018)2 0955-20960.

[36] J.H. Park, D.J. Min,H.S. Song, ISIJ Int., 42 (2) (2002) 127-131.

[37] J.H. Park,D.J. Min, ISIJ Int., 44 (2) (2004) 223-228.

[38] J.H. Park, G.H. Park,Y.E. Lee, ISIJ Int., 50 (8) (2010) 1078-1083.

[39] M. Fang, C.H. Lu, L.Q. Huang, H.X. Lai, J. Chen, J.T. Li, W.H. Ma, P.F. Xing,X.T. Luo, Sep. Sci. Technol., 49 (14) (2014) 2261-2270.

[40] J. Cai, J.T. Li, W.H. Chen, C. Chen,X.T. Luo, T. Nonferr. Metal. Soc., 21 (6) (2011) 1402-1406.

[41] L.A.V. Teixeira, K. Morita, ISIJ Int., 49 (6) (2009) 783-787.

PROCENA KARBIDNOG KAPACITETA ZA PROCESE RAFINACIJE U TROJNIM SISTEMIMA ŠLJAKE NA BAZI CaO PRI TEMPERATURI OD 1773K

Z.-G. Yu [a], H.-Y. Leng [a], L.-J. Wang [b], K.-C. Chou [a,*]

[a] Glavna državna laboratorija za napredni specijalni čelik & Glavna laboratorija za naprednu ferometalurgiju u Šangaju & Fakultet za inženjerstvo i nauku o materijalima, Univerzitet u Šangaju, Šangaj, Kina
[b] Glavna državna laboratorija za naprednu metalurgiju &Kolaboracioni inovativni centar za tehnologiju čelika, Univerzitet nauke i tehnologije u Pekingu, Peking, Kina

Apstrakt

Rafinaciona šljaka ima široku primenu u proizvodnji legura sa visokom dodatom vrednošću, kao i u proizvodnji posebnih vrsta čelika. Uklanjanje primesa zavisi od prenosa mase između graničnih površina šljake i metala, i karbidni kapacitet rafininacione šljake je od izuzetne važnosti za kontrolu sadržaja ugljenika u finalnim proizvodima. U ovom radu je uveden fenomenološki model za izračunavanje karbidnog kapaciteta u različitim trojnim sistemima rafinacione šljake na bazi CaO. Konturne linije karbidnog kapaciteta u CaO-Al_2O_3-CaF_2, CaO-SiO_2-CaF_2, i CaO-SiO_2-MnO sistemima su izračunate na osnovu ograničenih eksperimentalnih podataka u sadašnjem modelu. Eksperimentalni podaci unutar granica proračuna upoređeni su sa predviđenim vrednostima i primećeno je zadovoljavajuće slaganje sa prosečnom devijacijom od 1.4%, 2.3% i 1.6%, pojedinačno, za ova tri sistema. Sadašnji model je moćan i fleksibilan za proračunavanje karbidnog kapaciteta u trojnim sistemima šljake na bazi CaO, i može se primeniti i na druge sisteme.

Ključne reči*: Karbida kapacitet; Predviđanje; Model; Na bazi CaO; Rafinisana šljaka*